Journal of Solid State Chemistry 183 (2010) 1359–1364

Contents lists available at ScienceDirect

Journal of Solid State Chemistry

journal homepage: www.elsevier.com/locate/jssc

Photo-degradation of methylene blue using Ta-doped ZnO nanoparticle

Ji-Zhou Kong, Ai-Dong Li *, Xiang-Yu Li, Hai-Fa Zhai, Wen-Qi Zhang, You-Pin Gong, Hui Li, Di Wu

National Laboratory of Solid State Microstructures, Materials Science and Engineering Department, Nanjing University, Nanjing 210093, PR China

ARTICLE INFO

Article history:
Received 8 October 2009
Received in revised form
26 February 2010
Accepted 4 April 2010

Keywords:
1 mol % Ta-doped ZnO
Photocatalytic performance
Methylene blue dye
Absorption model

ABSTRACT

A photocatalyst of Ta-doped ZnO was prepared by a modified Pechini-type method. The structural, morphological properties and photocatalytic activity of 1 mol % Ta-doped ZnO samples annealed at different temperatures were characterized. The photo-oxidation of methylene blue under the visible-light irradiation followed the pseudo-first-order kinetics according to the Langmuir–Hinshelwood model. It is found that the photocatalysis of 1% Ta-doped ZnO annealed at 700 °C showed excellent performance of the photodegradation of methylene blue, which was attributed to a competitive trade-off among the crystallinity, surface hydroxyl groups, and specific surface area. The processing parameter such as the pH value also played an important role in tuning the photocatalytic activity. The maximum photodecomposed rate was achieved at pH = 8, and an novel model about the absorption of methylene blue on the surface of the catalysts was proposed.

1. Introduction

In recent years, nano-structured ZnO has attracted a great deal of attention, owing to its unique and novel applications in the optics, optoelectronics, catalysis, pyroelectricity and piezoelectricity [1]. Among these properties, the degradation of the pollutants catalyzed by ZnO has been studied widely [2–7]. ZnO is known to be one kind of the important photocatalysts because of its unique advantages, such as its low price, high photocatalytic activity, and nontoxicity. However, the disadvantage of this catalyst is that its catalytic activity is still not high enough for the commercial applications. An effective and practical approach to improve the photocatalytic property is doping by adding some heteroelements, because the material performances are mainly determined by the chemical properties of the atoms or ions and of the bonds between them. The presence of the doping metal ions in the ZnO crystalline matrix significantly affects the photocatalytic activity, charge carrier recombination rate and interfacial electron-transfer rate [8]. Generally speaking, the metal ions used as dopants are often the transition metal ions, e.g., Co^{2+} [9–11], Mn^{2+} [11,12], Mn^{4+} [13], Ti^{4+} [14], La^{3+} [15], Fe^{3+} [16] and so forth. Recently, several groups have discovered high photocatalytic activities for the decomposition of water in some tantalates and niobates [17]. Zou et al first reported that the direct splitting of water under the visible-light irradiation with $InTaO_4$ as photocatalyst of [18]. Kudo and Kato et al studied the photocatalytic properties of some alkaline and alkaline-earth tantalates and niobates, including $Sr_2Ta_2O_7$, $Sr_2Nb_2O_7$, and $NaTaO_3$ [17,19]. However, to date, most synthesis of powders of the tantalates and niobates have been carried out by the conventional solid-state reaction route at high temperature treatment (typically 1000–1300 °C).

In this work, the photoinduced degradation of methylene blue (MB) using the Ta-doped ZnO samples prepared by a modified Pechini-type method and annealed at different temperatures was investigated in depth. The impact of processing parameters such as the pH values during the photocatalytic reaction was also examined. The possible photocatalytic mechanism in Ta-doped ZnO systems was proposed. The imaginable absorption model of MB on the surface of the catalysts was first proposed, which explains why the catalysts showed better catalytic performance at the alkaline condition, than that at the acidic condition.

2. Preparation of catalyst

2.1. Materials

All chemicals were analytical grade and used without further purification. The synthesis of the home-made water-soluble peroxo-citrato-tantalum was described elsewhere in details [20]. Deionized water was used as the dispersing agent through all the experiments. MB was the commercial product which could be utilized in the photocatalytic oxidation and adsorption experiments.

2.2. Preparation of the catalyst

A modified Pechini-type method was used to prepare the Ta-doped ZnO powders [21]. The resultant dark grey glassy resin

* Corresponding author. Fax: +86 25 83595535.
E-mail address: adli@nju.edu.cn (A.D. Li).

0022-4596/$ - see front matter © 2010 Elsevier Inc. All rights reserved.
doi:10.1016/j.jssc.2010.04.005

finally underwent a two-step heat treatment to yield the final products: firstly pyrolysis at 400 °C for 2 h and then annealed at 500, 600, 700, 800 and 900 °C for 1 h in air, respectively.

2.3. Characterization of the catalyst

The structure of the powders was characterized by a powder X-ray diffraction (XRD) equipment (D/max 2000, Rigaku) using Cu $K\alpha$ radiation. The Ta-doping content of the samples was determined by the inductively coupled plasma resonance (ICP, JY 38 S, JY). The specific surface area (BET) was measured by the surface area apparatus (Micromeritics TriStar 3000, Shimadzu), using N_2 adsorption/desorption method at liquid nitrogen temperature (−196 °C). The microstructure of particles was analyzed by transmission electron microscopy (TEM, Tecnai G^2 F20 S-Twin, FEI). The X-ray photoelectron spectroscopy (XPS) measurements were performed on a Thermo ESCALAB 250 spectrophotometer with Al $K\alpha$ radiation ($h\nu$=1486.6 eV). The binding energies were calibrated with respect to the signal from the adventitious carbon (binding energy=284.8 eV). Relative quantitative analysis was carried out using the sensitivity factors supplied by the instrument.

2.4. Photocatalytic measurement

For the photocatalysis, all of the experiments were carried out under the similar conditions in the aqueous solution containing MB. The photocatalytic reaction system consisted of a Xe arc lamp (300 W, Ushio) located at 10 cm away from the reaction solution, with a cut-off filter providing the visible light ($\lambda \geq 420$ nm) and a water filter preventing from the thermal catalytic effect (the average temperature 25 ± 1 °C). 50 ml MB solution (10 mg/L) with 50 mg of catalyst was magnetically stirred before and during the illumination. The suspension was agitated for 30 min in the absence of the light, prior to the illumination, in order to achieve the maximum adsorption of the dye on the surface of the catalysts. The pH value of the samples was adjusted, prior to the tests, by adding 0.01 mol/L HCl or 0.01 mol/L NaOH solutions. The degradation process was monitored by a UV–vis–NIR spectrophotometer (UV-3600, Shimadzu; measuring the maximum absorption of MB at 664 nm).

The photodegradation rate could be calculated by $D(\%)=100\times(C_0-C_t)/C_0$, in which C_0 was the concentration of MB before the reaction, and C_t was the equilibrium concentration of MB after the irradiation time "t".

3. Results and discussion

3.1. Structure and morphology of Ta-doped ZnO

Fig. 1 shows the effect of the Ta doping content on the photocatalytic activity of Ta-doped ZnO annealed at 700 °C for 1 h. It can be easily observed that the Ta doping in ZnO improves the activity of the photocatalyst significantly, and the Ta-doping content has been tuned to obtain the optimal photocatalytic property. According to our previous study, it is known that 1.0 mol % Ta-doped ZnO photocatalyst has the highest photocatalytic activity about the photo-oxidation of methylene blue under the visible-light irradiation, owing to the highest concentration of the surface hydroxyl groups and active defect sites (e.g. hydrogen-related defect), the largest specific surface area [21]. Therefore, our interests focus on 1 mol % Ta doped ZnO samples in this work. The ICP analysis was used to determine the Ta-doping content. The measured value of the molar ratio of Ta to Zn is 0.01:0.99 in 1 mol % Ta-doped ZnO sample, which is consistent with the nominal composition.

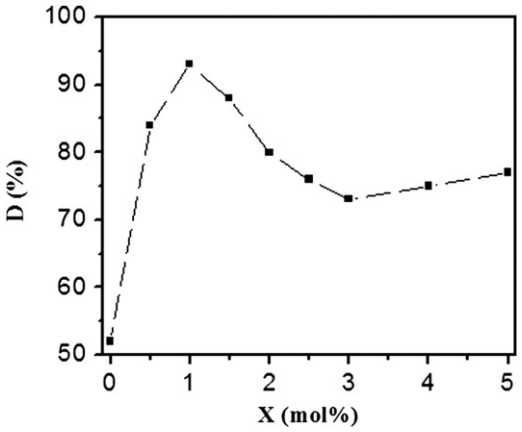

Fig. 1. Effect of the Ta-doping concentration of Ta-doped ZnO on the photocatalytic degradation of MB, t=40 min, pH=6.3.

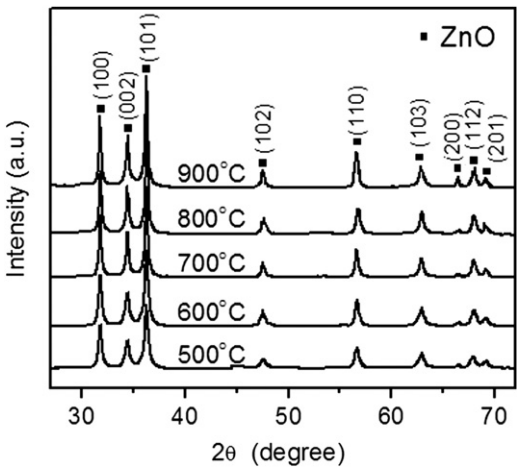

Fig. 2. XRD patterns of 1 mol % Ta-doped ZnO annealed at different temperatures.

The XRD patterns of 1 mol % Ta-doped ZnO annealed at different temperatures are shown in Fig. 2. All Ta-doped ZnO samples exhibited similar diffraction peaks from the hexagonal wurtzite ZnO (JCPDS card No. 75-0576) and no secondary phase containing Ta was detected which means that Ta^{5+} ion occupies the Zn^{2+} site to form the Ta-doped ZnO. The calculated unit parameter (c-axis) increases slightly from 5.194 to 5.199 Å due to the introduction of the larger Ta^{5+} ions. Another feature is that the full width at half maximum (FWHM) of the diffraction peaks becomes narrower gradually with increasing annealing temperature, indicating the better crystallinity at higher annealing temperature. Using the Scherrer equation, the average size of powders annealed at various temperatures was estimated, as listed in Table 1. The grain size increases from 19.7 to 35.6 nm, as the annealing temperature increases from 500 to 900 °C.

Table 1 also gives the specific surface areas of the Ta-doped ZnO annealed at different temperatures. As anticipated, the higher the annealing temperature is, the lower the specific surface area becomes. Both high specific surface area and good crystallinity are important to the photocatalytic activity. Therefore, a trade-off must be achieved between these two competitive factors.

The TEM image of the sample annealed at 700 °C is shown in Fig. 3a. Uniform and ultrafine 1 mol % Ta-doped ZnO nanoparticles with the average grain size of ~25.0 nm are observed in Fig. 3b,

Table 1
Grain size and specific surface area of 1 mol % Ta-doped ZnO annealed at various temperatures.

Annealed temperature (°C)	Particle size (nm)	Specific surface area (m^2/g)
500	19.7	40.6
600	21.2	39.3
700	23.5	36.1
800	28.3	27.3
900	35.6	21.2

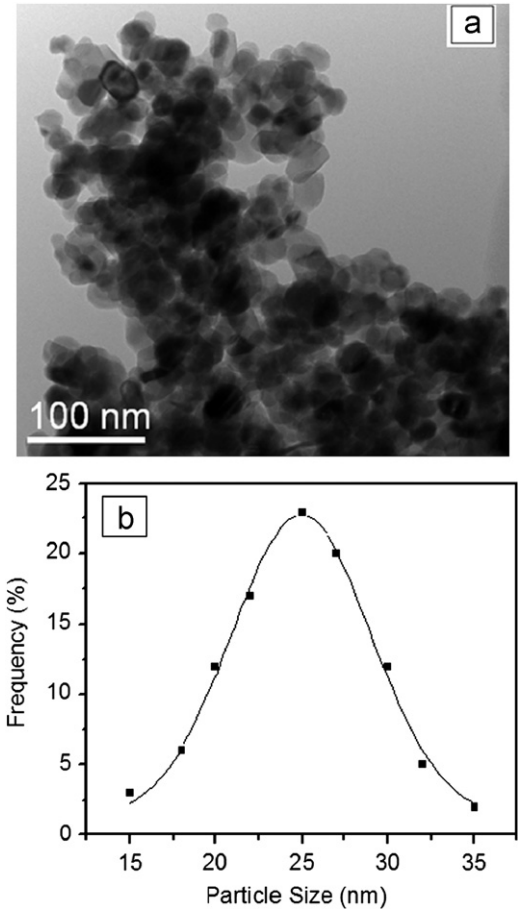

Fig. 3. (a) Representative TEM image of 1 mol % Ta-doped ZnO nanopowders annealed at 700 °C; (b) Particle size distribution. The measured data are fitted to Gaussian curve (solid line) with mean size of 25.0 nm, and the corresponding standard deviations is 7.8%.

which consisted with the calculated value of 23.5 nm from the Scherrer equation in Table 1. The standard deviations of 1 mol % Ta-doped ZnO nanoparticles is 7.8%, indicating a relatively narrow particle size distribution determined from the micrographs (See Fig. 3b). However, it appears the agglomerate phenomenon of nanoparticles because of the high temperature treatment.

The surface structures of 1 mol % Ta-doped ZnO annealed at 700 °C is also investigated by XPS, and the corresponding experimental results are shown in Fig. 4. The binding energies in the XPS spectra presented in Fig. 4 are calibrated by using that of C 1 s (284.8 eV). In Fig. 4a, the O 1 s profile is asymmetric and fitted with the non-linear least square fit program using Gauss–Lorentzian peak shapes. Three O 1 s peaks appear after deconvolution, indicating three different kinds of O species, located at 530.3, 531.8 and 533.2 eV, respectively. The low

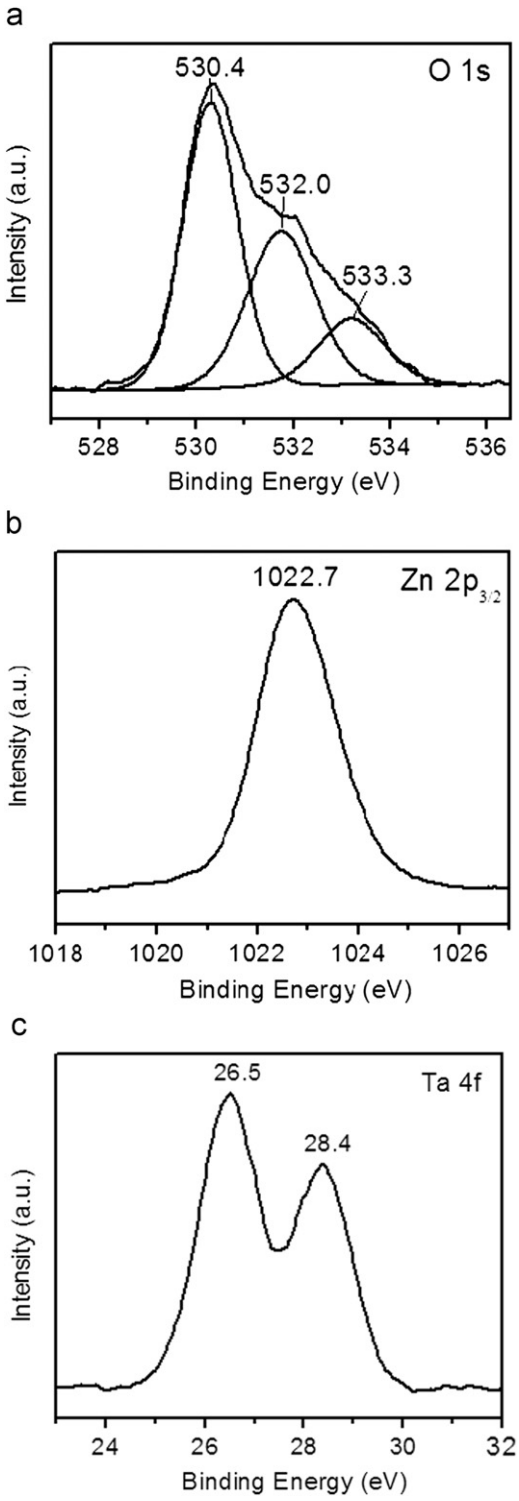

Fig. 4. XPS spectra of the ZnO nanopowders with the content of 1 mol % Ta annealed at 700 °C: (a) O 1 s spectrum XPS; (b) Zn $2p_{3/2}$ spectrum; and (c) Ta 4f spectra. The binding energies are calibrated using that of C 1 s (284.8 eV).

binding energy component centered at 530.3 eV can be ascribed to the O^{2-} ions in ZnO lattice (the lattice oxygen, O_L). The medium binding energy is related to specific chemisorbed adsorbed oxygen (O_S, 531.8 eV), caused by the surface adsorbed hydroxyl, H_2O, $-CO_3$ and so on in the samples [22]. Therefore, the physical adsorbed oxygen has little effect on this peak, since it is inclined to be desorbed in the high-vacuum environment. The component with the high binding energy centered at 533.2 eV is attributed to

the O^{2-} ions in the oxygen-deficient regions within the matrix of ZnO [23]. As a result, changes in the intensity of this component may be connected with the variations in the concentration of the oxygen vacancies ($V_o^{\bullet\bullet}$). The calculated ratio of the adsorption oxygen to the lattice oxygen (O_S/O_L) is 1:1.49. In addition, it is interesting to find that, with the addition of Ta, the binding energy of O 1 s peaks for the ZnO sample with a Ta-doping content of 1 mol % shifts remarkably to the higher binding energy, compared with the corresponding values of the standard binding energy of O 1 s in pure ZnO. The symmetric peak appeared at 1022.7 eV in Fig. 4b is attributed to Zn $2p_{3/2}$. Ta 4f core level spectra (Fig. 4c) exhibits two peaks centered at 28.4 and 26.5 eV, which can be assigned to $4f_{5/2}$ and $4f_{7/2}$ core levels of Ta^{5+}, respectively. According to the principle method and handbook of the XPS instrument, the relatively quantitative analysis can be performed basing on the XPS peak area of different elements and the corresponding sensitivity factor. The calculated proportion of Zn, Ta and lattice O on the surface of the sample is 1:0.09:1.06. Thus, some important XPS data could be obtained. The percentage of oxygen vacancies is 16.5%, which reveals the abundant oxygen vacancies in our samples are in good agreement with our previous study [21]. The oxygen vacancies are very active, so that they can lightly combine with other atoms or groups to be stable. It might mean that the 1% Ta doping in ZnO introduces enough quantities of active and valid defect sites to act as a key role in photodegradation process.

3.2. Photocatalytic activity and mechanism

It can be observed from Fig. 1 that 1 mol % Ta-doped ZnO shows the highest photocatalytic activity in all samples with various Ta doping contents. In fact, the annealing temperature is also an important factor to the photocatalytic efficiency. The photocatalytic activity of the samples annealed at various temperatures has been investigated. MB was adopted to evaluate the photocatalytic performance. As shown in Fig. 5, 1 mol % Ta-doped ZnO annealed at 700 °C exhibits the highest photocatalytic degradation rate. If the annealing temperature is lower than 700 °C, the photocatalytic activity of the catalysts increases gradually with the annealing temperature. If the annealing temperature is higher 700 °C, the photocatalytic activity decreases with the increasing of temperature. The photocatalytic efficiencies of 1 mol % Ta-doped ZnO annealed at various temperatures, named as 1% Ta-ZnO-T (T: the annealing temperatures) for short, are ranked in order from the highest to the lowest: 1% Ta-ZnO-700 > 1% Ta-ZnO-800 > 1% Ta-ZnO-900 > 1% Ta-ZnO-600 > 1% Ta-ZnO-500.

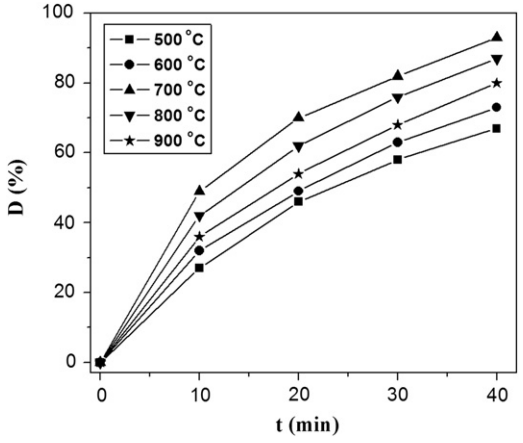

Fig. 5. Photodegradation efficiency of MB solution as function of the irradiation time for 1 mol % Ta-doped ZnO annealed at different temperatures, pH = 6.3.

There exist several competitive factors, such as the crystallinity, surface $^{\bullet}OH$ groups and specific surface area, varying with the annealing temperature [24]. As the annealing temperature increases, the crystallinity is improved with a loss of surface $^{\bullet}OH$ groups and specific surface area. It has been also reported that excessive quantities of hydroxyl groups on the catalyst surface have detrimental effect on photocatalytic oxidation, but small quantities are essential for sustained reaction rate [25]. Therefore, the highest photocatalytic activity has been achieved at annealing temperature of 700 °C, which is attributed to a competitive trade-off among the preferable crystallinity, optimal quantity of hydroxyl groups on the catalyst surface, and large enough specific surface area. It seems that the crystallinity predominate, compared with other two factors.

Under the visible light irradiation, an electron-hole pair forms, and then a conduction-band electron and a valence-band hole separate on the surface of catalyst. Maybe the hole permits the direct oxidation of organic dye to reactive intermediates. In the presence of the dissolved O_2, electrons from the photoexcited Ta-doped ZnO produce superoxide anion radicals O_2^-, which subsequently could generate H_2O_2 and $HO^{\cdot\cdot}$ radicals [26–29]. The high oxidative potential of the holes can form very reactive hydroxyl groups through decomposing of water. The active oxygen vacancies that severed as electron acceptors can trap the photo-induced electrons temporarily to restrain the surface recombination of photogenerated electrons and holes, and then attack the dissolved O_2 to yield surface-bound superoxide anion radicals O_2^- or hydroxyl groups, which can act as effective centers of organic matter mineralization for photocatalytic reactions [8].

The high oxidative potential of the hole (h^+) in the catalyst can form very reactive hydroxyl groups by the decomposition of water as well as the reaction of the holes with OH^-. Maybe the hole permits the direct oxidation of organic dye to reactive intermediates. Catalyst suspensions are particularly efficient photocatalytic systems for generating H_2O_2, due to the presence of hole scavengers such as formates, oxalates, acetates, amides, citrates and alcohols (organic species, generally) [28]. The photocatalytic reactions give birth to $^{\bullet}OH$ groups, which further promote the decomposition and eventually the total mineralization of the organic dye such as MB.

3.3. Kinetic study

According to many previous researches, the influence of the initial concentration of the solution on the photocatalytic degradation rate of the most organic compounds is described by the pseudo-first order kinetics, which is rationalized in terms of the Langmuir–Hinshelwood model, modified to accommodate reactions occurring at a solid–liquid interface [30,31]. The photocatalytic decolorization of MB using Ta-doped ZnO obeys the pseudo-first-order kinetics. At low initial dye concentration, the simplest representation for the rates of photodegradation of MB is given by

$$\ln C_t = -kt + \ln C_0 \quad (1)$$

This equation can be used to demonstrate linearity of data, if the integration of Eq. (1) is given by

$$\ln(C_0/C_t) = kt \quad (2)$$

where k is the constant of the pseudo-first-order rate.

A plot of $\ln(C_0/C_t)$ versus the visible irradiation time for the MB photo-decolorization catalyzed by 1% Ta-doped ZnO is shown in Fig. 6. A linear relation between $\ln(C_0/C_t)$ and the irradiation time has been confirmed, which implies the photodegradation of MB

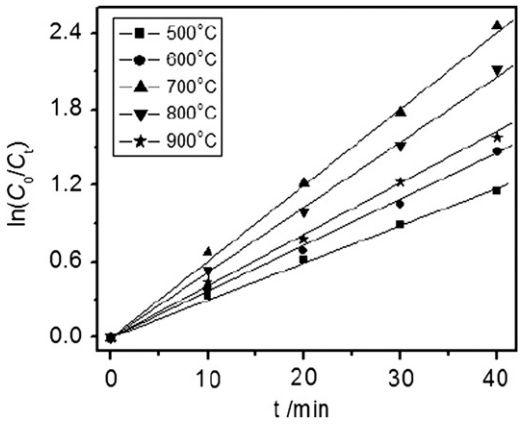

Fig. 6. Kinetic fit for the photodegradation of MB catalyzed by 1 mol % Ta-doped ZnO annealed at different temperatures, pH=6.3.

Table 2
First-order-rate constant (k) and half life ($t_{1/2}$) in the presence of 1 mol % Ta-doped ZnO annealed at different temperatures, pH=6.3.

Annealed temperature (°C)	k (min^{-1})	$t_{1/2}$ (min)
500	1.85×10^{-2}	37.4
600	2.46×10^{-2}	28.2
700	4.01×10^{-2}	17.2
800	3.34×10^{-2}	20.7
900	2.60×10^{-2}	26.7

follows the first-order kinetics with the catalyst of 1% Ta-doped ZnO. The obtained first-order rate constant (k) and half-life ($t_{1/2}$) have been listed in Table 2, which reveal a significant and favorable effect of Ta-doped ZnO on the photocatalytic removal of MB dye. The higher the first order rate constant is, the more outstanding the photocatalytic performance is. The k and $t_{1/2}$ for 1 mol % Ta-doped ZnO annealed at 700 °C, showing the excellent photocatalytic activity, are equal to $4.01\times10^{-2}\,min^{-1}$ and 17.2 min, respectively.

3.4. Effect of the pH value

Owing to the amphoteric behavior of most semiconductor oxides, the pH value, which also affects the photocatalytic process of various pollutants, is an important parameter in the reaction taking place on the semiconductor particle surface [30,32,33]. The role of pH value on the rate of the photocatalytic degradation was studied in the pH range of 5–12 at the constant dye concentration (10 mg/L) and catalyst amount (1.0 g/L) with the irradiation time of 20 min. The rate of dye degradation for the catalyst suspension at various pH values is plotted in Fig. 7a. In the illuminated Ta-doped ZnO system, the degradation rate of the dye is higher in the alkaline condition with almost two-fold enhancement as pH increases from 5 to 8. At pH=8, the maximum degradation rate is achieved. With the further increasing of pH values, the photodegradation rate of the organic dye becomes lower gradually.

The adsorption of H_2O molecules at surface metal sites is followed by the dissociation of OH^- groups, leading to coverage with chemically equivalent metal hydroxyl groups (M–OH) [33]. The followed equilibriums between the amphoteric behavior of most metal hydroxides and the acidic and alkali behavior of MB solution are considered as

$$M-OH+H^+ \rightarrow M-OH-H^+ \rightarrow M-H_2O^+ \quad (3)$$

$$M-OH+OH^- \rightarrow M-O^- + H_2O \quad (4)$$

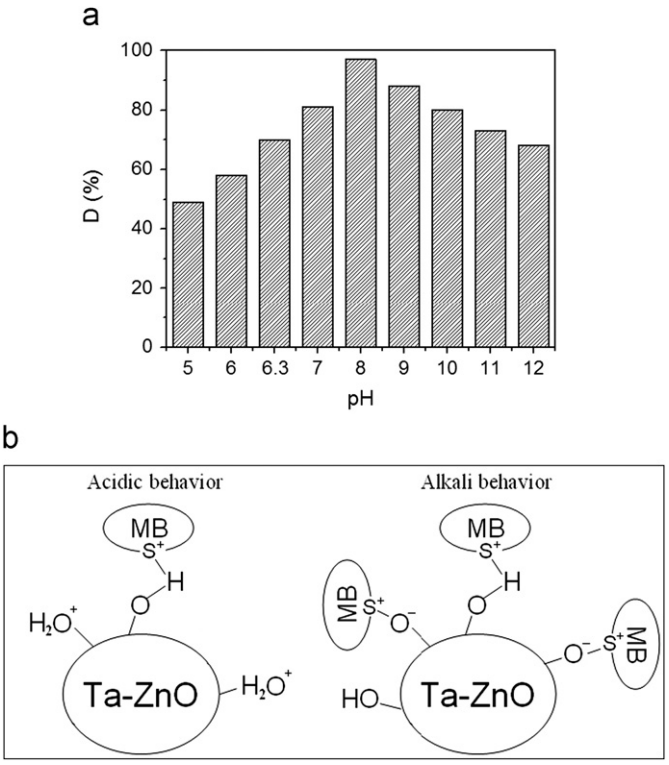

Fig. 7. (a) Effect of pH value on the photodegradation efficiency of MB solution in the presence of 1% Ta-doped ZnO annealed at 700 °C, t=20 min; (b) Model of the absorption of MB on the surface of the catalyst.

In different pH ranges, there exist electrostatic interactions (attraction or repulsion) between the catalyst surface and the organic molecules, which consequently enhance or inhibit the photodegradation rate, respectively. The effect of pH value on the photocatalysis is generally regarded as a result of the surface charge of Ta-doped ZnO and the relation with the ionic form of the organic compound (anionic or cationic). Fig. 7b shows the model of MB adsorption on the catalyst surface at the acidic and alkali condition. The low initial reaction rates at the acidic pH values are due to dissolution and photo-dissolution of ZnO [29]. Since MB is a kind of cationic compound, the observed increasing of the decomposition rate at low alkali pH can be attributed to the high hydroxylation of the catalyst surface, due to the presence of a large quantity of the hydroxyl groups. The higher concentration of the $^{\bullet}OH$ species are formed and the photodegradation reaction rate is then enhanced. Consequently, in high pH range, electrostatic attraction between the catalyst surface and the dye cations leads to a strong adsorption of the dye cations on the metal oxide support. At high alkali pH, although electrostatic attraction is improved, the hydroxyl groups decrease simultaneously. The decline of the reaction rates is ascribed to the breakage of the hydroxylation of the catalyst surface.

4. Conclusion

In summary, the Ta-doped ZnO nanoparticles were first prepared by a modified Pechini-type method. The ZnO sample with 1 mol % Ta-doping concentration exhibited the highest photocatalytic degradation rate under the visible light irradiation. A systematic study of the structural, morphological, and visible photocatalytic properties of 1 mol % Ta-doped ZnO samples annealed at different temperatures were investigated by various analytical techniques. The photo-oxidation followed the first

order kinetics according to the Langmuir–Hinshelwood model. It is found that 1% Ta-doped ZnO annealed at 700 °C shows excellent photocatalytic performance. This is attributed to a trade-off among crystallinity, surface hydroxyl groups, and specific surface area. The processing parameter such as pH value also played an important role in tuning the photocatalytic efficiency. The maximum photocatalytic degradation rate was achieved at pH=8. Thus the Ta-doped ZnO is a promising photocatalyst in large-scale utilization under visible light irradiation to photo-decompose water contamination and environmental pollution.

Acknowledgment

This project was supported by the Natural Science Foundation of China (10704035, 50932001 and 10974085) and a grant from the State Key Program for Basic Research of China (2006CB921805, 2009ZX02039-004 and 2009CB929500). Aidong Li also thank the support from the program for the "333" Talents in Jiangsu Province and SRF for ROCS, SEM.

References

[1] Z.L. Wang, J. Phys.: Condens. Mater. 16 (2004) 829–858.
[2] F. Xu, P. Zhang, A. Navrotsky, Z.Y. Yuan, T.Z. Ren, M. Halasa, B.L. Su, Chem. Mater. 19 (2007) 5680–5686.
[3] C. Hariharan, Appl. Catal. A: Gen. 304 (2006) 55–61.
[4] F. Lu, W.P. Cai, Y.G. Zhang, Adv. Funct. Mater. 18 (2008) 1047–1056.
[5] R. Comparelli, E. Fanizza, M.L. Curri, P.D. Cozzi, G. Mascolo, A. Agostiano, Appl. Catal. B: Environ. 60 (2005) 1–11.
[6] A. Akyol, H.C. Yatmaz, M. Bayramoglu, Appl. Catal. B: Environ. 54 (2004) 19–24.
[7] H.Q. Liu, J.X. Yang, J.H. Liang, Y.X. Huang, C.Y. Tangz, J. Am. Chem. Soc. 91 (2008) 1287–1291.
[8] G. Marci, V. Augugliaro, M.J. Lopez-Munoz, C. Martin, L. Palmisano, V. Rives, M. Schiavello, R.J.D. Tilley, A.M. Venezia, J. Phys. Chem. B 105 (2001) 1033–1040.
[9] P. Mahata, G. Madras, S. Natarajan, J. Phys. Chem. B 110 (2006) 13759–13768.
[10] X.Q. Qiu, G.S. Li, X.F. Sun, L.P. Li, X.Z. Fu, Nanotechnology 19 (2008) 215703.
[11] S. Ekambaram, Y. Iikubo, A. Kudo, J. Alloy Compd. 433 (2007) 237–240.
[12] R. Ullah, J. Dutta, J. Hazard. Mater. 156 (2008) 194–200.
[13] S.J. Li, Z.C. Ma, J. Zhang, J.Z. Liu, Catal. Commun. 9 (2008) 1482–1486.
[14] Q. Zhang, W. Fan, L. Gao, Appl. Catal. B: Environ. 76 (2007) 168–173.
[15] S. Anandan, A. Vinu, K.L.P.S. Lovely, N. Gokulakrishnan, P. Srinivasu, T. Mori, V. Murugesan, V. Sivamurugan, K. Ariga, J. Mol. Catal. A: Chem. 266 (2007) 149–157.
[16] D. Li, H. Haneda, J. Photochem. Photobiol. A: Chem. 160 (2003) 203–212.
[17] H. Kato, A. Kudo, J. Phys. Chem. B 105 (2001) 4285–4292.
[18] Z.G. Zou, J.H. Ye, K. Sayama, H. Arakawa, Nature 414 (2001) 625–627.
[19] A. Kudo, H. Kato, S. Nakagawa, J. Phys. Chem. B 104 (2000) 571–575.
[20] A.D. Li, J.Z. Kong, H.F. Zhai, J.B. Chen, D. Wu, J. Am. Ceram. Soc. 92 (9) (2009) 1959–1965.
[21] J.Z. Kong, A.D. Li, H.F. Zhai, Y.P. Gong, D. Wu, J. Solid State Chem. 182 (8) (2009) 2061–2067.
[22] Y.H. Zheng, L. Zheng, Y.Y. Zhan, X.Y. Lin, Q. Zheng, K. Wei, Inorg. Chem. 46 (2007) 6980.
[23] X.Q. Wei, B.Y. Man, M. Liu, C.S. Xue, H.Z. Zhuang, C. Yang, Phys. B: Condens. Mater. 388 (2007) 145–152.
[24] S.Y. Kim, T.H. Lim, T.S. Chang, C.H. Shin, Catal. Lett. 117 (2007) 112–118.
[25] L.X. Cao, A.M. Huang, F.J. Spiess, S.L. Suib, J. Catal. 188 (1999) 48–57.
[26] J.R. Harbour, M.L. Hair, J. Phys. Chem. 83 (1979) 652–656.
[27] V. Kandavelu, H. Kastien, K.R. Thampia, Appl. Catal. B: Environ. 48 (2004) 101–111.
[28] C. Kormann, D. Bahnemann, M.R. Hoffmann, Environ. Sci. Technol. 22 (1988) 798–806.
[29] I. Poulios, A. Avranas, E. Rekliti, A. Zouboulis, J. Chem. Technol. Biotechnol. 75 (2000) 205–212.
[30] C.S. Turci, D.F. Ollis, J. Catal. 122 (1990) 178–192.
[31] A.B. Prevot, M. Vincenti, A. Bianciotto, E. Pramauro, Appl. Catal. B: Environ. 22 (1999) 149–158.
[32] S. Sakthivel, B. Neppolian, M.V. Shankar, B. Arabindoo, M. Palanichamy, V. Murugesan, Sol. Energy Mater. Sol. Cells 77 (2003) 65–82.
[33] M.M. Uddin, M.A. Hasnat, A.J.F. Samed, R.K. Majumdar, Dyes Pigm. 75 (2007) 207–212.